Research in Astron. Astrophys. Vol.0 (200x) No.0, 000–000
http://www.raa-journal.org *http://www.iop.org/journals/raa*

***R**esearch in*
***A**stronomy and*
***A**strophysics*

arXiv:1603.04988v1 [astro-ph.GA] 16 Mar 2016

Observational evidence for the evolution of nuclear metallicity and star formation rate as the merger stage

Rui Guo[1,2,3], Cai-Na Hao[3], Xiao-Yang Xia[3], Peng Wei[2,4] and Xin Guo[3]

[1] National Astronomical Observatories, Chinese Academy of Sciences, 20A Datun Road, Chaoyang District, Beijing 100012, China
[2] University of Chinese Academy of Sciences, Beijing 100049, China
[3] Tianjin Astrophysics Center, Tianjin Normal University, Tianjin 300387, China; *E-mail: cainahao@gmail.com*
[4] School of Astronomy and Space Science, Nanjing University, Nanjing 210093, China

Abstract We investigate the evolution of nuclear gas-phase oxygen abundance and star formation rate (SFR) of local far-infrared selected star-forming galaxies along the merger sequence, as traced by their optical morphologies. The sample was drawn from a cross-correlation analysis of the *IRAS* Point Source Catalog Redshift Survey and 1 Jy ultraluminous infrared galaxies sample with the Sloan Digital Sky Survey Data Release 7 database. The investigation is done by comparing our sample to a control sample matched in the normalized redshift distribution in two diagnostics, which are the nuclear gas-phase metallicity vs. stellar mass and the nuclear SFR vs. stellar mass diagrams. Galaxies with different morphological types show different mass-metallicity relations (MZR). Compared to the MZR defined by the control sample, isolated spirals have comparable metallicities with the control sample at a given stellar mass. Spirals in pairs and interacting galaxies with projected separations $r_p > 20$ kpc show mild metallicity dilution of 0.02-0.03 dex. Interacting galaxies with $r_p < 20$ kpc, pre-mergers and advanced mergers are under-abundant by ~ 0.06, ~ 0.05 and ~ 0.04 dex, respectively. This shows an evolutionary trend that the metallicity is increasingly depressed as the merging proceeds and it is diluted most dramatically when two galaxies are closely interacting. Afterwards, the interstellar medium (ISM) is enriched when the galaxies coalesce. This is the first time that such ISM enrichment at the final coalescence stage is observed, which demonstrates the importance of supernova explosion in affecting the nuclear metallicity. Meanwhile the central SFR enhancement relative

to the control sample evolves simultaneously with the nuclear gas-phase oxygen abundance. Our results support the predictions from numerical simulations.

Key words: galaxies: abundances — galaxies: evolution — galaxies: interactions — galaxies: starburst — galaxies: star formation — infrared: galaxies

1 INTRODUCTION

Chemical abundance is a record of the history of galaxy formation. Stellar mass and chemical abundance, two of the most fundamental properties of galaxies, were found to be correlated: for star-forming galaxies, the correlation between stellar mass and nuclear gas-phase oxygen abundance exists from z=0 up to z > 3, with more massive galaxies being more metal rich (e.g., Lequeux et al. 1979; Garnett & Shields 1987; Tremonti et al. 2004, T04 hereafter; Erb et al. 2006; Sanders et al. 2015; Maiolino et al. 2008; Mannucci et al. 2009). Galaxy interactions and mergers, however, may not follow the trend because tidal interactions can change the chemical properties of galaxies significantly. In the past decade, several studies have found that the central metallicities of local interacting and merging systems are under-abundant by ~ 0.05 dex on average or even up to 0.3-0.4 dex for merging systems with high star formation rates such as ultraluminous infrared galaxies (ULIRGs; with infrared luminosity $L_{\rm IR}$[1]$> 10^{12} L_{\odot}$), compared to isolated galaxies with comparable stellar masses (e.g., Kewley et al. 2006, Michel-Dansac et al. 2008; Rupke et al. 2008; Ellison et al. 2008; Peeples et al. 2009; Alonso et al. 2010). This chemical dilution was interpreted as a result of gas inflows from the outer part of the galaxy induced by galaxy interactions and mergers.

To understand the influence of galaxy interactions and mergers on the nuclear metallicity in depth, numerical simulations were employed (Rupke et al. 2010; Montuori et al. 2010; Perez et al. 2011; Torrey et al. 2012). These simulations demonstrated that inflows of gas triggered by tidal interactions can dilute the central metallicity. But they also revealed that other physical processes, such as chemical enrichment from star formation, outflows of gas triggered by stellar and AGN feedback etc, take effect as well. Although different authors used different prescriptions of star formation, metal enrichment, feedback, model galaxy set-up etc, a coherent picture was obtained. When two gas-rich galaxies approach, tidal torques remove the angular momentum of gas in the outer part of the galaxy and funnel it into the galaxy center. The inflows of these metal-poor gas dilute the central metallicities, as well as enhance the central star formation activities. Afterwards, the following stellar winds and supernova explosion eject metals into the interstellar medium (ISM) and make the ISM enriched. Meanwhile, stellar winds and supernova explosion prevent gas cooling and blow away gas and metals, which depress star formation activities and metal enrichment. These authors found that there are two dilution peaks,

[1] $L_{\rm IR}$ is the integrated infrared luminosity between 8-1000 μm.

one following the first pericentric passage and the other preceding the final coalescence. The under-abundance of the dilution peaks is significant, $\sim 0.2 - 0.4$ dex. For evolutionary stages in between, the metallicity depression is mild. The ISM enrichment is most pronounced at the final coalescence stage, within physical separations less than 4 kpc (Montuori et al. 2010). Star formation rate (SFR) enhancement follows a similar variation pattern, and the SFR peaks are almost synchronous with the dilution peaks, with a delay no more than 10^8 yr.

To find observational evidences for the variations of metallicity and star formation rate as the merger stages, Scudder et al. (2012) studied the metallicity dilution and star formation rate enhancement as a function of the projected separations r_p, based on a sample of 1899 galaxies in pairs drawn from Sloan Digital Sky Survey (SDSS) Data Release 7 (DR7). By comparing to the control sample matched in stellar mass, redshift and density for each galaxy in a pair, they found that the gas-phase oxygen abundances of galaxies in pairs are depressed by 0.02 dex on average within $r_p = 60\,h_{70}^{-1}\,\mathrm{kpc}$ and the amplitude of depression increases as r_p decreases. The SFRs are found to be enhanced out to $r_p = 80\,h_{70}^{-1}\,\mathrm{kpc}$ with a trend of increasing enhancement at decreasing separations, by an amount of 0.21 dex within $r_p = 30\,h_{70}^{-1}\,\mathrm{kpc}$ and 0.11 dex in the range of $30 - 80\,h_{70}^{-1}\,\mathrm{kpc}$ on average. Such trends are demonstrated to be qualitatively consistent with the simulations except for the ISM enrichment after the final coalescence stage which was not covered in their study. Ellison et al. (2013) added post-mergers, which are galaxies at the final coalescence stage, to the merger sequence. But they found that the metallicity in post-mergers is even more depressed than that in the closest pairs. We note that the projected separation was used as an indicator of the merger stages in Scudder et al. (2012) and Ellison et al. (2013), whereas galaxies with the same projected separations may be experiencing different merger stages (Montuori et al. 2010). As pointed out by Scudder et al. (2012), apart from the projected separation, morphological disturbance of a galaxy can be used to trace the merger phase as well. Despite its drawbacks as an observable indicator of merger states (Scudder et al. 2012), the morphology can serve as a complement to the projected separation. Moreover, Torrey et al. (2012) suggested that morphologically classified merger stages or IR luminosity/SFR divided samples may be more suitable for such studies. Most recently, Kilerci Eser et al. (2014) studied the metallicity and SFR distributions as a function of morphologically classified evolutionary stages for a sample of ULIRGs but they did not find significant difference in the distributions of both gas-phase oxygen abundances and SFRs for galaxies at different merger stages. They ascribed this to the statistics that may smooth out the evolution of oxygen abundances and SFRs of individual ULIRGs. We suspect that ULIRGs may not consist of the whole merger sequence of galaxies since most galaxies involved in interactions or mergers are not so luminous as ULIRGs in the IR. The incomplete merger sequence probed by ULIRGs only may account for the findings that ULIRGs at different stages do not show considerable differences in the distributions of oxygen abundances and SFRs. Therefore galaxy samples with

a wider range of IR luminosities and morphological information may provide a better testbed for such studies.

In this paper, we select a galaxy sample from a cross-correlation between the *Infrared Astronomical Satellite (IRAS)* Point Source Catalog Redshift (PSCz) survey (Saunders et al. 2000) and 1 Jy ULIRGs sample (Kim & Sanders 1998) with SDSS DR7 (York et al. 2000; Abazajian et al. 2009). Our galaxy sample covers a broad range of IR luminosity ($10^{10} - 10^{12.5}\,L_{\odot}$) and is classified morphologically based on the optical images provided by SDSS to trace the interaction stages. Using this sample, the variations of nuclear gas-phase oxygen abundances and SFRs along the merger sequence are re-visited. The paper is organized as follows. In Sections 2 and 3, we describe our sample selection and parameter estimations, respectively. We present the results in Section 4. The findings are discussed in Section 5 and summarized in Section 6. Throughout this paper, we adopt the Kroupa (2001) initial mass function (IMF) and a cosmology with $H_0 = 70\,\mathrm{km\,s^{-1}Mpc^{-1}}$, $\Omega_{\mathrm{m}} = 0.3$ and $\Omega_{\Lambda} = 0.7$.

2 SAMPLE

2.1 Selection of the Working Sample

The aim of this paper is to investigate the possible evolution of the nuclear gas-phase oxygen abundance and SFR as merger stages, based on a sample of galaxies with optical imaging and spectroscopic data along with measurements of IR luminosities. In this subsection we describe the selection procedure for our working sample.

To minimize the probability of mismatching, we used the *IRAS* PSCz catalog and 1 Jy ULIRGs sample, both of which provide spectroscopic redshifts and optical positions, to cross-correlate with the spectroscopic catalog of SDSS DR7 for the selection of our working sample. The selection criteria are described below.

Firstly, we searched the spectroscopic catalog of SDSS DR7 for counterparts of objects with optical positions in *IRAS* PSCz using a $5''$ matching radius and 0.001 redshift differences. In consideration of reliable morphological classification and sample completeness (Fukugita et al. 2004, Kauffmann et al. 2003b), we constrained our sample galaxies to a *r*-band Petrosian magnitude range of 14.5 to 15.9 mag after corrections for foreground Galactic extinction (Schlegel et al. 1998) following Wang et al. (2006). This yielded 644 galaxies[2] with $L_{\mathrm{IR}} > 10^{10} L_{\odot}$. We note that for a galaxy in a pair or interacting system, the observed *IRAS* far-infrared (FIR) fluxes are probably contributed by the whole system because of the large *IRAS* beam size of $\sim 3'$. However, companions with separations larger than $5''$ have been missed by our $5''$ matching radius. To maximize our sample size, we searched for companions of these

[2] The *r*-band image of Q08510+0055 has several columns of bad pixels across the galaxy, making it difficult to be morphologically classified. The [NII] and Hα flux measurements of Q12116+5448 have some problems. So we removed them from our sample.

644 galaxies from the spectroscopic Catalog of SDSS DR7 by requiring a projected separation $r_p < 80\,\mathrm{kpc}$ and $\Delta v < 500\,\mathrm{km\,s^{-1}}$. Only the nearest companion was selected. This resulted in 98 companions, out of which 30 companions have *r*-band Petrosian magnitudes within the range of 14.5-15.9 mag. We added these 30 galaxies to our sample. In addition, we note that only three ULIRGs are included in the *r*-band magnitude constrained sample. In order to include more ULIRGs in our sample, we performed a cross-correlation between the *IRAS* 1Jy sample and the spectroscopic catalog of SDSS DR7. From this cross-identification, we obtained another 37 ULIRGs[3] and added them to our sample. Since these ULIRGs are obvious interacting or merging systems, we did not restrict their *r*-band magnitudes to the magnitude range of 14.5-15.9 mag. In total we obtained 711 FIR-selected galaxies.

Secondly, we examined the location of SDSS fibers on the optical images for our sample galaxies. For 32 galaxies, the spectra were taken for the off-center regions of the galaxies. To ensure the reliability of the central metallicity and SFR measurements, we excluded these galaxies. This reduced our sample to 679 galaxies.

Finally, we separated star-forming galaxies from AGNs. To ensure a reliable spectral type classification, we removed galaxies with emission line signal-to-noise ratios (S/N) less than 5. According to the commonly used BPT diagnostic diagram (Baldwin et al. 1981) developed by Kauffmann et al. (2003a) based on [OIII] $\lambda5007$/Hβ versus [NII] $\lambda6584$/Hα, we selected 343 star-forming galaxies, among which five are ULIRGs.

Figure 1 shows the distributions of redshifts and total infrared luminosities[4] of the 343 FIR-selected star-forming galaxies. The majority of the sample has $z < 0.1$ and $10^{10} L_\odot < L_{\mathrm{IR}} < 10^{12.5} L_\odot$.

2.2 Morphological Classification

To characterize the merger stages of our FIR-selected star-forming galaxies, we classified them into the following seven morphological categories:

- S: Isolated normal spiral galaxies without bars.
- SB: Isolated barred spiral galaxies.
- Edge-on: Isolated galaxies with high-inclination angles.
- Pair: Galaxies with companions within $r_p < 80\,\mathrm{kpc}$, $\Delta v < 500\,\mathrm{km\,s^{-1}}$ but not disturbed morphologically.

[3] Two 1Jy ULIRGs are already included in the *IRAS* PSCz catalog. So they are not counted here.

[4] For galaxies with companions, we cannot distinguish their contributions to the IR emission. So we simply assigned the IR luminosities of the system to both of them and keep in mind that their intrinsic IR luminosities are lower than those we plotted.

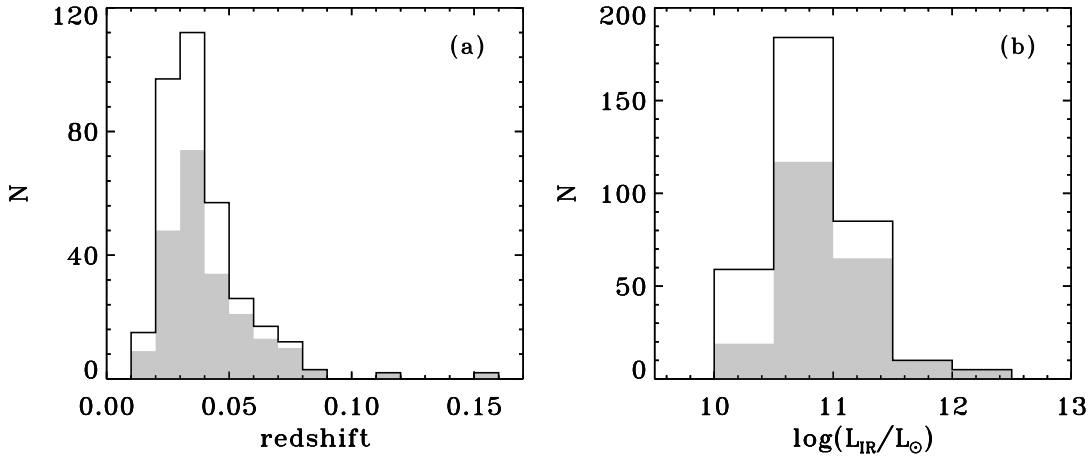

Fig. 1 Redshift and infrared luminosity distributions. The black histograms denote the 343 FIR-selected star-forming galaxies from the cross-correlation analysis (see Section 2.1), while the gray shaded histograms represent the 216 sample galaxies with morphological types of isolated spirals, spirals in pairs, close interacting, wide interacting, pre-merger and adv-merger used in this work (see Section 2.2).

– Interacting: Galaxies with companions within $r_p < 80\,\mathrm{kpc}$, $\Delta v < 500\,\mathrm{km\,s^{-1}}$ and morphologically disturbed.

– Pre-merger: Galaxies with two or more nuclei and sharing a common envelope.

– Adv-merger: Galaxies with only one nucleus but with some merger features, such as tidal tails.

In practice, we first classified pair and interacting galaxies. They are defined as systems that consist of two galaxies with a projected separation $r_p < 80\,\mathrm{kpc}$ and $\Delta v < 500\,\mathrm{km\,s^{-1}}$. For the galaxies that do not have a companion in the spectroscopic catalog, as described in Section 2.1, we searched for their companions from the photometric Catalog of SDSS DR7. If a galaxy has a companion in the photometric catalog with $r_p < 80\,\mathrm{kpc}$, we retrieved the redshift of the companion from the NED website[5] to identify physical pairs with a criterion of $\Delta v < 500\,\mathrm{km\,s^{-1}}$. For all galaxies with a true companion that was identified either from the spectroscopic or the photometric catalog, we classified them into pairs or interacting galaxies judging by their morphological disturbances in the SDSS *r*-band images. Galaxies in pairs were then further classified into spirals, barred-spirals and edge-on galaxies. Interacting galaxies were divided into wide interacting and close interacting galaxies using the projected separation

[5] http://ned.ipac.caltech.edu/

Table 1 Morphological classification of FIR-selected star-forming galaxies as a function of $L_{\rm IR}$

	$\log L_{\rm IR}/L_{\odot}$					
Morphology	10.0-10.5	10.5-11.0	11.0-11.5	11.5-12.0	12.0-12.5	Total
S	4	40	14	1	0	59
pair_S	0	17	6	2	0	25
inter>20kpc	3	12	10	2	0	27
inter<20kpc	3	6	10	1	1	21
pre-merger	5	2	5	0	2	14
adv-merger	4	40	20	4	2	70
Total	19	117	65	10	5	216

of $20\,{\rm kpc}$ as the dividing point[6] according to Kewley et al. (2006; see also Montuori et al. 2010). For the remaining sample galaxies, we visually classified them into the other five categories judging by their appearances in the SDSS *r*-band images. The composite (*g*-, *r*-, *i*- band) true color images (Lupton et al. 2004) were used as cross-check.

In order to estimate the reliability of our morphological classifications, we examined the consistency of our results with the classifications from Galaxy Zoo 1[7]. The Galaxy Zoo project performed visual morphological classifications for SDSS galaxies (Lintott et al., 2008; Lintott et al., 2011). For each galaxy, people are asked to vote for the most likely morphological category of this galaxy, out of Elliptical, ClockWise spirals, AntiClockWise spirals, Edge-on spirals, Merger and Combined Spiral (CS=Edge+CW+ACW). According to the vote fractions of each category, the galaxy is divided into one of the three broad classes: elliptical, spiral and unknown. To compare with the classifications from Galaxy Zoo, we considered our isolated S and SB as Spiral, our interacting, pre-merger and adv-merger as Merger. The comparison shows that our classifications for spiral galaxies are consistent with those of Galaxy Zoo but 36 (10%) mergers in our sample are denoted as spiral or elliptical galaxies by Galaxy Zoo. However, these 36 galaxies do show signs of disturbances, except one galaxy that we have not come to an agreement. After discussion, we modified the classification of this galaxy according to the result of Galaxy Zoo, and kept our results for the rest ones.

There are also 37 galaxies with morphologies not belonging to any categories defined above. They are ellipticals, blue compact drawfs, irregulars or have morphologies that we cannot classify without doubt. We do not consider them in the following analyses. In addition, we

[6] We tested with $30\,{\rm kpc}$ and $10\,{\rm kpc}$ as the dividing point to separate the wide from the close interacting galaxies and found that the median metal under-abundance and median SFR enhancement only change by a small amount. Therefore, our results are not sensitive to the selection of the dividing point.

[7] http://data.galaxyzoo.org/

removed barred-spirals in both isolation and pairs from our sample since bar instabilities can change both metallicity and star formation rate (e.g., Ellison et al. 2011 and references therein; Martel et al. 2013; Cacho et al. 2014). On the other hand, dust attenuation in edge-on galaxies cannot be corrected well, so we further excluded the edge-on galaxies from the following analysis. This resulted in a total number of 216 sample galaxies with morphological types of isolated spiral, spiral in pairs, wide interacting galaxy, close interacting galaxy, pre-merger and adv-merger making up an evolutionary sequence of galaxy mergers. The numbers of galaxies within each morphological category and IR luminosity range for our final sample are listed in Table 1. As can be seen from Table 1, the number of pre-mergers is 14. Results shown by pre-mergers may be biased due to the small sample size and thus will not be taken seriously. The shaded histograms in Figure 1 show the distributions of redshift and total infrared luminosities of the final galaxy sample.

2.3 Selection of the Control Sample

Apart from exploring the variations of the nuclear gas-phase oxygen abundance and SFR as merger stages within the FIR-selected sample, we need to determine their absolute offsets with respect to non-FIR-selected galaxies with comparable stellar mass. So a control sample of star-forming galaxies without IR constraints is also required.

The control sample was selected from the spectroscopic catalog of SDSS DR7. We first constrained the foreground Galactic extinction corrected Petrosian *r*-band magnitudes to the range of $14.5 < r < 17.77$ to meet the completeness limit of the spectroscopic selection (Strauss et al. 2002; Kauffmann et al. 2003b; Brinchmann et al. 2004). Star-forming galaxies were then extracted according to the BPT diagram, as mentioned in Section 2.1. Finally, we selected our control sample galaxies randomly from these star-forming galaxies by requiring their normalized redshift distribution to match with that of the working sample as shown in the left panel of Figure 1. The purpose of matching the normalized redshift distribution is to minimize the aperture effect caused by the fixed $3''$ fiber aperture adopted by the SDSS spectroscopic observations (Kewley et al. 2005). Our final control sample is composed of 44484 star-forming galaxies.

3 ESTIMATION OF PHYSICAL PARAMETERS

In this section we describe our methods of estimating the total stellar masses, the nuclear gas-phase oxygen abundances and SFRs.

The stellar masses were retrieved from the Max Planck Institute for Astrophysics-Johns Hopkins University (MPA/JHU[8]) stellar mass catalog. A Bayesian analysis was employed to estimate the stellar masses by comparing a large number of stellar population synthesis models

[8] http://www.mpa-garching.mpg.de/SDSS

with the five broad-band *u, g, r, i, z* photometry of SDSS. The stellar population synthesis models include both bursting and continuous star formation histories, which properly sampled the real star formation histories of galaxies (Kauffmann et al. 2003b). We note that the stellar masses of pre-mergers are probably under-estimated because the photometry performed by the SDSS pipeline only measures the fluxes of part of the system.

The nuclear gas-phase oxygen abundances were retrieved from the MPA/JHU gas-phase metallicity catalog. As described in T04, the gas-phase oxygen abundances were determined by fitting the stellar population synthesis and photo-ionization models developed by Charlot & Longhetti (2001; see also Brinchmann et al. 2004) to optical nebular emission lines in SDSS spectra.

Instead of extracting nuclear SFRs directly from the MPA/JHU catalog, Hα luminosities were used to calculate the instantaneous nuclear SFRs. We first extracted the Hα emission line fluxes in the SDSS 3″ fiber aperture from the MPA/JHU catalog. We then performed internal extinction corrections for the Hα fluxes by assuming the case B recombination value of intrinsic Hα/Hβ as 2.86 and using O'Donnell (1994) Milky Way extinction curve. The internal extinction corrected Hα luminosities were then used to calculate the central SFRs following Kennicutt (1998). Kennicutt (1998)'s prescription was built on a Salpeter (1955) IMF. To derive SFRs under an assumption of a Kroupa IMF, we divided the SFRs by a factor of 1.5. We note that the dust attenuations derived from Balmer decrement may be under-estimated for galaxies with very dusty star formation (e.g., Kennicutt et al. 2009; Kilerci Eser et al. 2014). So the dust-corrected SFRs for these galaxies may be under-estimated, which should be kept in mind when the variations of SFRs as merger states are examined (Section 4.2).

4 RESULTS

4.1 Metallicity Dilution

We first examine the location of our FIR-selected galaxies in the mass-metallicity diagram by comparing them with the mass-metallicity relation defined by the control sample of non-FIR-selected star-forming galaxies.

The mass-metallicity relation defined by our control sample is derived using a method similar to the bisector of linear fitting. We first divide the control sample into 25 subgroups by their stellar masses with binwidth of 0.1 dex from $8.5 < \log M_* < 11.0$ and obtain the median metallicity of galaxies in each subgroup. Then these 25 pairs of data points ($\log M_*$, $12 + \log(O/H)$) are fitted to a polynomial with the form:

$$12 + \log(O/H) = a + b(\log M_*) + c(\log M_*)^2. \quad (1)$$

Afterwards, a similar fitting is performed for the median stellar masses of galaxies in subgroups split by their metallicities with a binwidth of 0.05 dex from $8.2 < 12 + \log(O/H) < 9.2$. We

then generate a list of data points from these two curves and fit these data points to a polynomial with the form of Equation (1). The derived bisector-like mass-metallicity relation is

$$12+\log(O/H) = -5.588(\pm0.514)+2.586(\pm0.107)(\log M_*)-0.11283(\pm0.00561)(\log M_*)^2, \quad (2)$$

and it is extrapolated to $\log M_* = 11.2$ to cover the stellar mass range probed by our FIR-selected star-forming galaxies.

Figure 2(a) shows the distributions of our FIR-selected star-forming galaxies in the gas-phase oxygen abundance vs. stellar mass diagram. The data points are color-coded by their IR luminosities. The black solid curve represents the mass-metallicity relation defined by the control sample, i.e., Equation (2). The contours indicate the 68%, 95% and 99% level number densities of the control sample galaxies. From this panel, we can see that the FIR-selected star-forming galaxies roughly follow the mass-metallicity relation of normal star-forming galaxies with a majority (87%) of them lying within the 95% ($\sim 2\sigma$) level number density contour, but show a slight systematic shift towards lower abundance. We further find that the galaxies with IR luminosities greater than $10^{11} L_{\odot}$ (the orange, magenta and red points) are more massive and more metal-poor than those with lower IR luminosities. It is expected that IR more luminous galaxies are more massive according to the well-known stellar mass – total SFR relation, i.e., the star-forming "main sequence" (e.g., Brinchmann et al. 2004; Elbaz et al. 2007). The trend that IR more luminous galaxies are more metal-poor was also reported in Rupke et al. (2008). They suggested that this trend is related to the large fractions of later-stage mergers and higher SFRs in LIRGs and ULIRGs. In Figure 2(b)-(g), we plot our sample galaxies with different morphologies separately. Specifically, we show isolated spirals, spirals in pairs, wide and close interacting galaxies, pre-mergers and adv-mergers. To our surprise, the systematically larger under-abundance of LIRGs and ULIRGs is not caused by the larger fractions of interacting galaxies and mergers in them. Except for close interacting galaxies, within all the other morphological categories, LIRGs and ULIRGs are more metal-poor than IR less luminous galaxies with the same morphological type, including isolated spirals. We speculate that larger amount of gas in LIRGs and ULIRGs (e.g., Gao & Solomon 2004) is responsible for the larger under-abundance, which is also expected in numerical simulations (e.g., Perez et al. 2011). The panels (b)-(g) of Figure 2 show that the positions of our FIR-selected galaxies evolve with the merger stages, as probed by the optical morphologies, in the metallicity vs. stellar mass diagram. Compared to the control sample, isolated spirals and wide interacting galaxies are around the relation. But spirals in pairs, close interacting galaxies, pre-mergers and adv-mergers show obvious under-abundance and the amount of the under-abundance evolves with the merger phase.

In order to measure the evolution of the under-abundance more quantitatively, we plot the histograms of the offsets in the gas-phase oxygen abundances from the mass-metallicity relation in Figure 3. The distribution of the offsets for all 216 FIR-selected star-forming galaxies

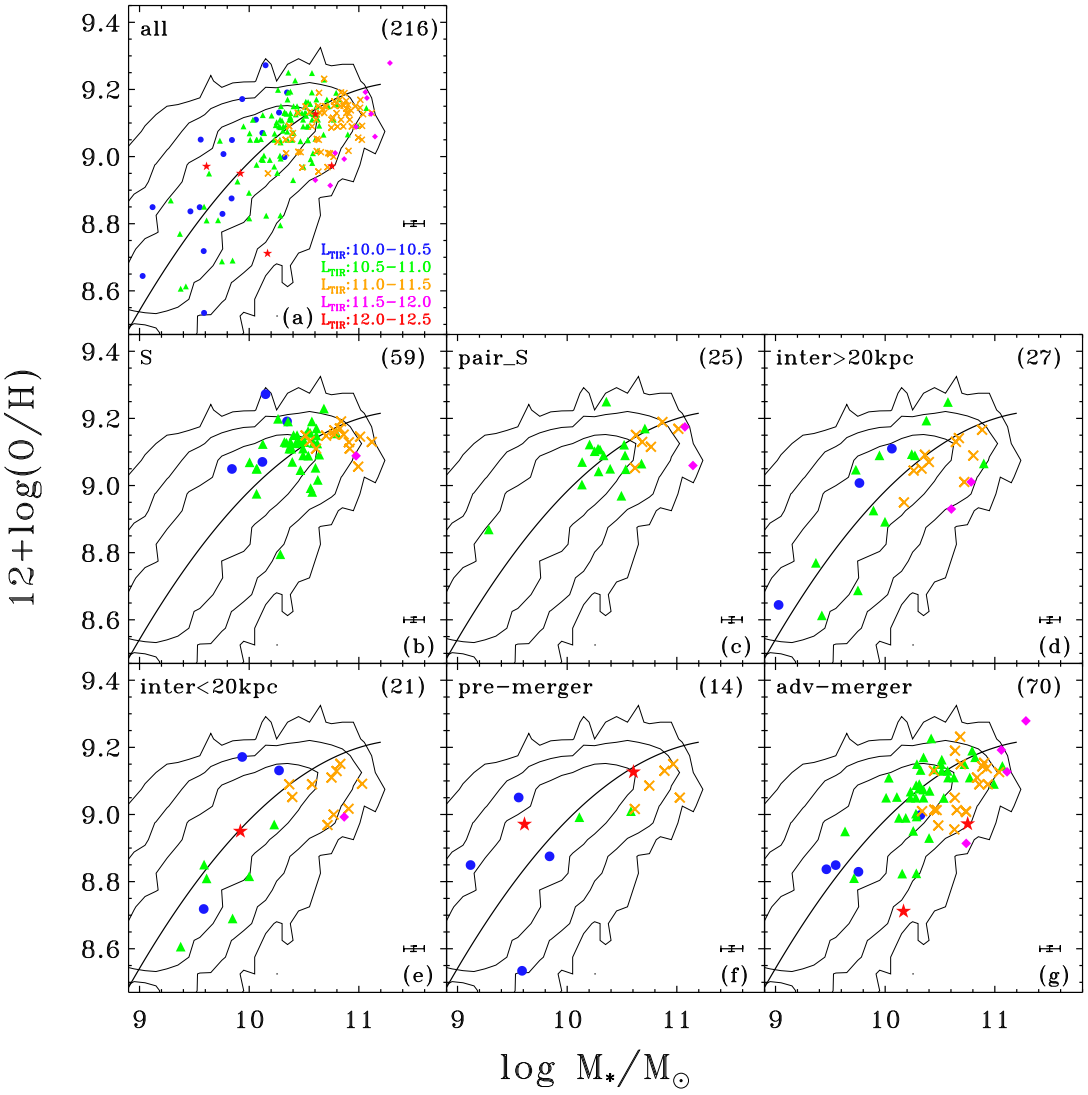

Fig. 2 Nuclear gas-phase oxygen abundance versus stellar mass relation. Symbols with different colors represent our sample galaxies within different infrared luminosity ranges. The black solid curves indicate the mean MZR defined by the control sample. The contours enclose 68%, 95% and 99% control sample galaxies, respectively. All the 216 sample galaxies are shown in panel (a). Isolated spirals, spirals in pairs, interacting galaxies with $r_p < 20$ kpc, $r_p > 20$ kpc, pre-mergers and adv-mergers are shown in panels (b)-(g) respectively. Morphological types and the corresponding galaxy numbers are indicated in each panel. The error bars show the median uncertainties.

is shown in Figure 3(a). On average, it shows an under-abundance of ~ 0.03 dex. The histogram for isolated spirals is shown in Figure 3(b) and it is plotted in the other panels as a reference (the gray shaded histogram). The panels (c)-(g) show the distributions of the offsets for galaxies with morphologies of spiral in pairs, wide interacting, close interacting, pre-merger and adv-merger, respectively. The median and mean values of the offsets, as labeled in each panel, provide consistent results for each morphological type within one rms scatter. The FIR-selected isolated spirals show no systematic offset from the mass-metallicity relation defined by the control sample. The systematic shifts of the empty histograms relative to the shaded histogram shown in the panels (b)-(g) tell a clear picture of metallicity evolution as galaxies interact and merge. Spirals in pairs and galaxies involved in wide interacting systems show a mild nuclear metallicity depression, $\sim$ 0.02-0.03 dex. As the merger progresses, the metallicities of galaxies in close interacting systems are diluted most dramatically, by $\sim$ 0.06 dex in median. When two galaxies merge together, the gas is enriched by $\sim 0.02 - 0.03$ dex, as can be seen from the comparison of the close interacting galaxies (dashed histogram) with the adv-mergers (the solid histogram) in Figure 3(g). Although the gas is enriched relative to the close interacting galaxies, the metallicity is still lower than the control sample, which is consistent with the predictions from numerical simulations (e.g., Torrey et al. 2012; Scudder et al. 2012). This is the first time that such relative enrichment at the final merger stage is seen from observations, which demonstrates the importance of the supernova feedback to the ISM enrichment at the coalescence stage of mergers. Apart from the evolutionary trend, we note the broad distribution of the offsets, which implies that the amount of metallicity dilution is also affected by many other factors, such as the orbital parameters, gas fractions etc, as suggested by numerical simulations (e.g., Montuori et al. 2010; Perez et al. 2011; Torrey et al. 2012).

Consistent with previous works, the amplitude of metallicity dilution or enrichment in this study is small. At the end of this subsection, we examine the statistical significance of the metallicity evolution by comparing the offsets with the error bars and via the K-S test with the distribution of isolated spirals. Since the method used to calculate the gas-phase metallicity for the working sample is the same as that for the comparison sample, systematic errors in different metallicity estimators are not important in our study. We only consider the mean random error of the gas-phase oxygen abundance measurements, which is $\sim$ 0.01 dex. The spirals in pairs and wide-interacting galaxies are under-abundant at 2σ levels while the K-S tests show insignificant difference from the isolated spirals with probabilities drawn from the same distribution of 37% and 11%, respectively. By contrast, the under-abundances in close-interacting galaxies and adv-mergers are significant at $> 3\sigma$ levels. Furthermore, the K-S tests indicate that the difference of the under-abundance of the close-interacting galaxies and the adv-mergers with respect to the isolated spirals is significant with probabilities drawn from the same distribution of 0.1% and 0.7%, respectively. The mean/median difference between close-interacting galaxies and adv-mergers is 0.03/0.02 dex, which is statistically significant

at $\sim 3\sigma/2\sigma$ levels. Therefore, the evolutionary trend of the metallicity under-abundance we saw above is statistically significant at $> 2\sigma$ levels, although the amplitude of the metallicity dilution is small.

4.2 Star Formation Rate Enhancement

Galaxy interactions and mergers not only affect the nuclear metallicity as shown in Section 4.1, but also influence the nuclear SFR. In this subsection, we examine the variation of the central SFR with the IR luminosity and morphology. Similar to what we performed for the study of the nuclear metallicity, we investigate the variation of the nuclear SFR in terms of the stellar mass – nuclear SFR relation.

We first obtain the stellar mass – nuclear SFR relation by an ordinary least squares bisector linear regression fitting based on our control sample. The best-fitting relation gives

$$\mathrm{SFR} = -11.67(\pm 0.034) + 1.11(\pm 0.004)(\log M_*). \quad (3)$$

We show the distributions of galaxies in the nuclear SFR vs. stellar mass diagram in Figure 4(a). Equation (3) is plotted as the straight solid line. The contours denote the 68%, 95% and 99% level number densities of the control sample galaxies. This panel shows that the galaxies follow the trend defined by the control sample but have systematically higher nuclear SFRs. It is also seen that IR more luminous galaxies are more massive, as we have seen in Figure 2(a). However, in contrast to the offsets in the gas-phase oxygen abundance, the nuclear SFR offsets with respect to the control sample do not vary with the IR luminosities. This seems to be conflicting with the studies on stellar mass – global SFR relation, which found that LIRGs and ULIRGs have much higher global SFRs than normal star-forming galaxies with comparable stellar mass (e.g., Elbaz et al. 2007; Kilerci Eser et al. 2014). However, considering that the dust-corrected SFRs for LIRGs and ULIRGs are possibly more severely under-estimated than the galaxies with lower IR luminosities because of their extremely dusty environment in the central regions (Sanders & Mirabel 1996; Lonsdale et al. 2006), as we have emphasized in Section 3, it is understandable that the IR more luminous galaxies do not show larger nuclear SFR offsets. For each morphological type, we examine the distributions of galaxies in the nuclear SFR vs. stellar mass diagram in Figure 4(b)-(g). We can see that regardless of their IR luminosities, isolated spirals and spirals in pairs follow the stellar mass – nuclear SFR relation defined by the control sample. The systematic enhancement exhibited in Figure 4(a) is caused by the obvious SFR enhancement in interacting galaxies and mergers, as shown in panels (d)-(g) of Figure 4.

Similar to Figure 3, we plot the histograms of the nuclear SFR offsets relative to the stellar mass – nuclear SFR relation defined by the control sample in Figure 5. The histogram for all 216 sample galaxies is plotted in Figure 5(a). They show a SFR enhancement of ~ 0.2 dex on average. Figure 5(b) shows the histogram for isolated spirals and this histogram is plotted

in the remaining panels as a reference. The panels (c)-(g) show the histograms of SFR enhancement for spirals in pairs, wide interacting, close interacting, pre-merger and adv-merger galaxies, respectively. The median and mean values of the enhancements, labeled in each panel, are coincident for each morphological type within one rms scatter except for the close interacting galaxies. The FIR-selected isolated spirals show a marginal SFR enhancement relative to the control sample by 0.07 dex in median. In contrast, spirals in pairs and wide interacting galaxies show a minor systematic shift (~ 0.1 dex) towards SFR enhancement while close interacting galaxies and adv-mergers show systematic shift towards the right most significantly by ~ 0.4 dex on average. K-S tests show that the distributions of SFR enhancement for spirals in pairs and wide interacting galaxies are not significantly different from the isolated spirals while close interacting galaxies and adv-mergers differ from the isolated spirals at significance levels greater than 99.9%. The SFR enhancement in pre-mergers may be biased due to the small sample size. We note that the enhancement in adv-mergers is slightly milder than close interacting galaxies in median but it is comparable to close interacting galaxies on average. K-S test suggests that these two distributions are similar at a significance level of 27.9%. Although the average offsets suggest SFR enhancements in our galaxies, the range of the offsets is large, varying from SFR depression (negative values) to SFR enhancement (positive values).

5 DISCUSSION

5.1 Sample Selection Biases

Our sample is obtained via a FIR-optical cross-correlation analysis and several criteria have been used to obtain the final sample (see Section 2.1). So it is worth investigating possible sample selection biases and their impact on the final results.

The goal of this paper is to explore the evolution of the nuclear gas-phase oxygen abundances and SFRs along the FIR-selected merger sequence by investigating their positions on the gas-phase oxygen abundance and SFR versus stellar mass diagrams. Therefore, any selection biases would not affect the final results as long as no biases are introduced into the morphological types and objects with certain values of stellar masses, gas-phase oxygen abundances and SFRs are not preferentially selected or missed. In other words, a representative sample for each morphological type is sufficient for this work.

During the sample selection process, three selection criteria could introduce biases into the sample. The first is the cross-identification of the IRAS PSCz and the spectroscopic catalog of SDSS DR7, from which galaxies under the IR detection limit are missed. And it is well known that a flux-limited sample misses objects with lower luminosities at higher redshift (i.e., the Malmquist bias), which results in a sample with more luminous galaxies occupying the higher redshift distribution and less luminous galaxies dominating the lower redshift distribution. The Malmquist bias would not affect our results due to the small coverage in redshift ($z < 0.1$

mostly; see Figure 1). FIR-selected samples are biased to galaxies which are more massive and are undergoing more rigorous star formation. However, this bias behaves similarly towards all morphological types in the sample. As a result, the evolutionary trend of the nuclear metallicity and SFR along the merger sequence, as characterized by morphological types, is not affected by this selection bias, although the absolute amplitudes of metal under-abundance and SFR enhancement relative to the control sample may be changed.

The second is the *r*-band magnitude cut – only galaxies with *r*-band Petrosian magnitudes within the range of 14.5-15.9 mag are included. As Wang et al. (2006) concluded, such magnitude cut does not introduce significant biases into the morphological types. The exclusion of galaxies with fainter *r*-band Petrosian magnitudes tends to remove galaxies with larger redshifts, higher IR luminosities and higher nuclear SFRs. However, similar to the first selection effect, this selection bias affects all morphological types in a similar way. Consequently, it may only affect the absolute amplitudes of metal depression and SFR enhancement but does not change the evolutionary trend with the merger stages.

The third is the requirement of the redshift measurements to identify objects within pairs. Apart from the spectroscopic catalog of SDSS DR7, NED was used to search for redshifts for candidate companions identified from the SDSS photometric catalog (see Section 2.2). There are fifteen isolated spirals with photometric companions that do not have spectroscopic redshift information. The *r*-band images of these fifteen companions show that most of them (12 out of 15) are probably background galaxies, suggested by their small sizes and faint brightness. So the requirement of the redshift measurements only affects the classification of three isolated spirals at most and it does not have selection effects in terms of stellar masses, metal abundances and SFRs.

To summarize, our sample is composed of representative samples of galaxies within each morphological type although it is not a complete sample. As a result, the sample selection biases mentioned above do not affect our main results significantly.

5.2 Comparisons with the Literature

Recently, Scudder et al. (2012) and Ellison et al. (2013) investigated the evolution of central metallicity and SFR along the merger sequence. Specifically, Scudder et al. (2012) studied galaxy pairs with stellar mass ratios of 0.1-10 and did not include galaxies at the final coalescence stage, while Ellison et al. (2013) studied major mergers (with stellar mass ratio of 0.25-4) and added post-mergers to the merger sequence. Given that our interacting galaxies and mergers are FIR-selected, which are expected to be mostly involved in major mergers, it is straightforward to compare our results with Ellison et al. (2013). Since the projected separation was used as an indicator of the merger states in Ellison et al. (2013), we cannot compare our results shown by each morphological type with those shown in their work. However, we can compare our close interacting galaxies with their pairs with $r_p < 20h^{-1}$kpc and our wide

interacting galaxies with their pairs with $r_p > 20h^{-1}$kpc. Our adv-mergers can be compared directly with their post-mergers.

In terms of gas-phase oxygen abundance, our results are consistent with Ellison et al. (2013) for both close pairs ($r_p < 20h^{-1}$kpc) and wide pairs ($r_p > 20h^{-1}$kpc). However, for galaxies at the final coalescence stage, Ellison et al. (2013) obtained different results from ours. They found that post-mergers are even more metal-poor than the closest pairs by ~ 0.02 dex in median while we found a relative metallicity enrichment of 0.02-0.03 dex in our adv-mergers with respect to the close interacting galaxies.

Regarding to SFR, our median SFR enhancement of wide interacting galaxies is smaller than that of wide pairs in Ellison et al. by ~ 0.1 dex. For close interacting galaxies, the average SFR enhancement shown by our sample are comparable to Ellison et al. but our median SFR enhancement is larger by an additional amount of ~ 0.2 dex. The SFR enhancement for post-mergers obtained by Ellison et al. are ~ 0.2 dex higher than our adv-mergers. In summary, Ellison et al. obtained an evolutionary trend that SFR enhancement increases all the way to the final coalescence stage as the merger proceeds, while we found that SFR flattens or even decreases when galaxies evolve to the adv-merger stage.

The difference between the evolutionary trend from close pairs to post-mergers found by Ellison et al. (2013) and that from interacting galaxies to the adv-mergers found in this work may imply that our adv-mergers are more evolved than the post-mergers in Ellison et al. (2013). So the ISM have more time to be enriched and the gas content is more consumed, which leads to a decrease in the SFR.

5.3 Co-evolution of Metallicity and SFR

As we have shown in Sections 4.1 and 4.2, both nuclear gas-phase oxygen abundance and SFR evolve along the merger sequence and the pattern of the evolution is consistent with numerical simulations. Montuori et al. (2010; see also Fig 8 of Torrey et al. 2012; Fig 11 of Scudder et al. 2012) pointed out that the maximum metallicity dilution occurs almost simultaneously with the most intensive star formation enhancement, with a delay of 100 Myrs at most. To compare with this theoretical prediction, we examine the evolution of the median metallicity dilution (top panel) and SFR enhancement (bottom panel) along the merger sequence in Figure 6. Since we could not trace each evolutionary stage as the simulations did, we only compare the evolutionary trend with that predicted by simulations in a broad sense. Figure 6 shows that the metallicity dilution and SFR enhancement evolve synchronously. As the merger proceeds, metallicity decreases and SFR increases and they reach their minimum and maximum respectively when the two galaxies are within 20 kpc. After the peaks, metallicity increases and SFR decreases. This evolutionary trend of both nuclear gas-phase oxygen abundance and SFR supports the predictions from numerical simulations (e.g., Torrey et al. 2012; Scudder et al. 2012).

6 SUMMARY

We have selected a sample of FIR-selected star-forming galaxies from a cross-correlation analysis of *IRAS* PSCz and 1 Jy sample with the spectroscopic catalog of SDSS DR7 and classified them into different morphological types. Only a sub-sample of 216 galaxies with morphologies of isolated spiral, spiral in pairs, wide interacting, close interacting, pre-merger and adv-merger is considered in this study. To re-visit the evolution of the nuclear metallicity dilution and SFR enhancement along the merger sequence, we examine the relative positions of the 216 galaxies with respect to a redshift-matched control sample on the stellar mass-metallicity and stellar mass-central SFR diagrams. We summarize our main results as follows.

1. We find that, compared to normal star-forming galaxies with comparable stellar mass, galaxies with larger infrared luminosities are more depressed in the gas-phase oxygen abundance, which may be resulted from the larger gas content in these galaxies.

2. When the optical morphologies are used as tracers of evolutionary stages, galaxies show evolution in their nuclear metallicities along the merger sequence. The central metallicities of isolated spirals are similar to the normal star-forming galaxies, while spirals in pairs and wide interacting galaxies with $r_p > 20$ kpc show mild metallicity dilution, $\sim$ 0.02-0.03 dex. As the merging proceeds, close interacting galaxies show the most depressed metallicity, $\sim$ 0.06 dex in median and the amplitude of the depression decreases when the galaxies merge together. This is the first time that such ISM enrichment in the final coalescence stage is seen from observations.

3. The central SFR enhancement shows a coherent evolutionary trend with the nuclear metallicity. SFR enhancement increases as the merger proceeds and reaches its maximum when two galaxies are closely interacting. Afterwards, the SFR flattens or decreases.

Our results support the evolutionary trend predicted by numerical simulations that the central metallicity will be diluted by the inflow gas during the interacting/merging process accompanied with the SFR enhancement and the ISM will be enriched by the supernova feedback at the final coalescence stage (Montuori et al. 2010; Perez et al. 2011; Torrey et al. 2012).

Acknowledgements We thank Dr. Gang Chen for helpful discussion. This project is supported by the NSF of China 11373027 and 11003015. The Project-sponsored by SRF for ROCS, SEM. Funding for the creation and distribution of the SDSS Archive has been provided by the Alfred P. Sloan Foundation, the Participating Institutions, the National Aeronautics and Space Administration, the National Science Foundation, the U.S. Department of Energy, the Japanese Monbukagakusho, and the Max Planck Society. The SDSS Web site is http://www.sdss.org/. The SDSS is managed by the Astrophysical Research Consortium (ARC) for the Participating

Institutions. The Participating Institutions are The University of Chicago, Fermilab, the Institute for Advanced Study, the Japan Participation Group, The Johns Hopkins University, the Korean Scientist Group, Los Alamos National Laboratory, the Max-Planck-Institute for Astronomy (MPIA), the Max-Planck-Institute for Astrophysics (MPA), New Mexico State University, University of Pittsburgh, Princeton University, the United States Naval Observatory, and the University of Washington.

References

Abazajian, K. N., Adelman-McCarthy, J. K., Agüeros, M. A., et al. 2009, ApJS, 182, 543

Alonso, M. S., Michel-Dansac, L., & Lambas, D. G. 2010, A&A, in press (arXiv:1001.4605)

Baldwin, J. A., Phillips, M. M., & Terlevich, R. 1981, PASP, 93, 5

Brinchmann, J., Charlot, S., White, S. D. M., et al. 2004, MNRAS, 351, 1151

Cacho, R., Sánchez-Blázquez, P., Gorgas, J., & Pérez, I. 2014, MNRAS, 442, 2496

Charlot, S., & Longhetti, M. 2001, MNRAS, 323, 887

Elbaz, D., Daddi, E., Le Borgne, D., et al. 2007, A&A, 468, 33

Ellison, S. L., Mendel, J. T., Patton, D. R., & Scudder, J. M. 2013, MNRAS, 435, 3627

Ellison, S. L., Nair, P., Patton, D. R., et al. 2011, MNRAS, 416, 2182

Ellison, S. L., Patton, D. R., Simard, L., & McConnachie, A. W. 2008, AJ, 135, 1877

Erb, D. K., Shapley, A. E., Pettini, M., et al. 2006, ApJ, 644, 813

Fukugita, M., Nakamura, O., Turner, E. L., Helmboldt, J., & Nichol, R. C. 2004, ApJ, 601, L127

Gao, Y., & Solomon, P. M. 2004, ApJ, 606, 271

Garnett, D. R., & Shields, G. A. 1987, ApJ, 317, 82

Kauffmann, G., Heckman, T. M., Tremonti, C., et al. 2003a, MNRAS, 346, 1055

Kauffmann, G., Heckman, T. M., White, S. D. M., et al. 2003b, MNRAS, 341, 33

Kennicutt, R. C., Jr. 1998, ARA&A, 36, 189

Kennicutt, R. C., Jr., Hao, C.-N., Calzetti, D., et al. 2009, ApJ, 703, 1672-1695

Kewley, L. J., Geller, M. J., & Barton, E. J. 2006, AJ, 131, 2004

Kewley, L. J., Jansen, R. A., & Geller, M. J. 2005, PASP, 117, 227

Kilerci Eser, E., Goto, T., & Doi, Y. 2014, ApJ, 797, 54

Kim, D.-C., & Sanders, D. B. 1998, ApJS, 119, 41

Kroupa, P. 2001, MNRAS, 322, 231

Lequeux, J., Peimbert, M., Rayo, J. F., Serrano, A., & Torres-Peimbert, S. 1979, A&A, 80, 155

Lintott, C., Schawinski, K., Bamford, S., et al. 2011, MNRAS, 410, 166

Lintott, C. J., Schawinski, K., Slosar, A., et al. 2008, MNRAS, 389, 1179

Lonsdale, C. J., Farrah, D., & Smith, H. E. 2006, Astrophysics Update 2 (Praxis Publishing Ltd, Chichester, UK), 285

Lupton, R., Blanton, M. R., Fekete, G., et al. 2004, PASP, 116, 133

Maiolino, R., Nagao, T., Grazian, A., et al. 2008, A&A, 488, 463

Mannucci, F., Cresci, G., Maiolino, R., et al. 2009, MNRAS, 398, 1915

Martel, H., Kawata, D., & Ellison, S. L. 2013, MNRAS, 431, 2560

Michel-Dansac, L., Lambas, D. G., Alonso, M. S., & Tissera, P. 2008, MNRAS, 386, L82

Montuori, M., Di Matteo, P., Lehnert, M. D., Combes, F., & Semelin, B. 2010, A&A, 518, A56

O'Donnell, J. E. 1994, ApJ, 422, 158

Peeples, M. S., Pogge, R. W., & Stanek, K. Z. 2009, ApJ, 695, 259

Perez, J., Michel-Dansac, L., & Tissera, P. B. 2011, MNRAS, 417, 580

Rupke, D. S. N., Kewley, L. J., & Barnes, J. E. 2010, ApJ, 710, L156

Rupke, D. S. N., Veilleux, S., & Baker, A. J. 2008, ApJ, 674, 172

Salpeter, E. E. 1955, ApJ, 121, 161

Sanders, D. B., & Mirabel, I. F. 1996, ARA&A, 34, 749

Sanders, R. L., Shapley, A. E., Kriek, M., et al. 2015, ApJ, 799, 138

Saunders, W., Sutherland, W. J., Maddox, S. J., et al. 2000, MNRAS, 317, 55

Schlegel, D. J., Finkbeiner, D. P., & Davis, M. 1998, ApJ, 500, 525

Scudder, J. M., Ellison, S. L., Torrey, P., Patton, D. R., & Mendel, J. T. 2012, MNRAS, 426, 549

Strauss, M. A., Weinberg, D. H., Lupton, R. H., et al. 2002, AJ, 124, 1810

Torrey, P., Cox, T. J., Kewley, L., & Hernquist, L. 2012, ApJ, 746, 108

Tremonti, C. A., Heckman, T. M., Kauffmann, G., et al. 2004, ApJ, 613, 898

Wang, J. L., Xia, X. Y., Mao, S., et al. 2006, ApJ, 649, 722

York, D. G., Adelman, J., Anderson, J. E., Jr., et al. 2000, AJ, 120, 1579

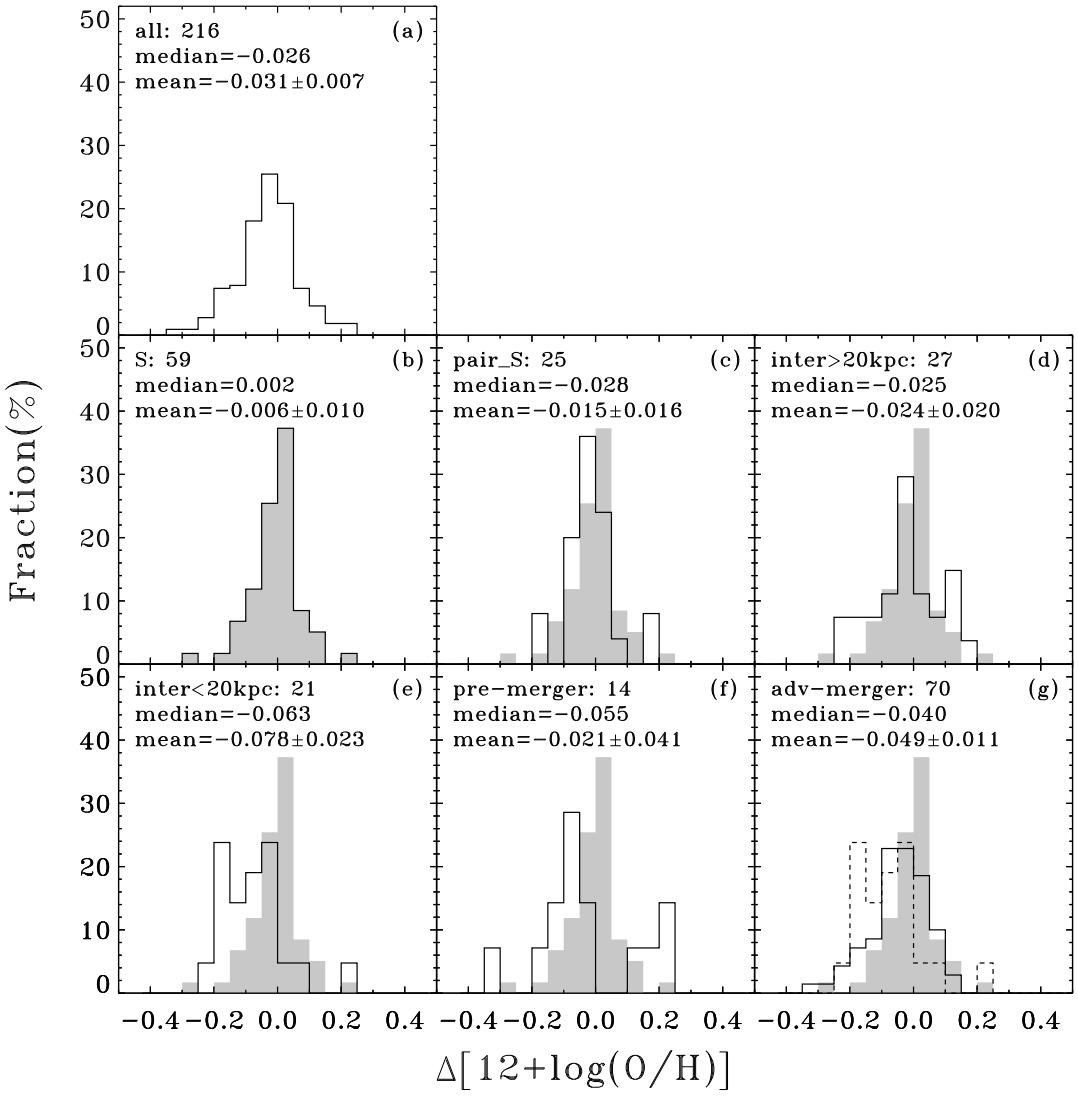

Fig. 3 Histograms of the nuclear metallicity offset with respect to the MZR relation defined by the control sample. In each panel, the black histogram denotes galaxies within each morphological category while the gray shaded histogram represents the histogram of isolated spiral galaxies for comparison. Morphological types, the corresponding galaxy numbers, the mean and median of the offsets are labeled in each panel. The dashed histogram in panel (g) represents the distribution for the close interacting galaxies.

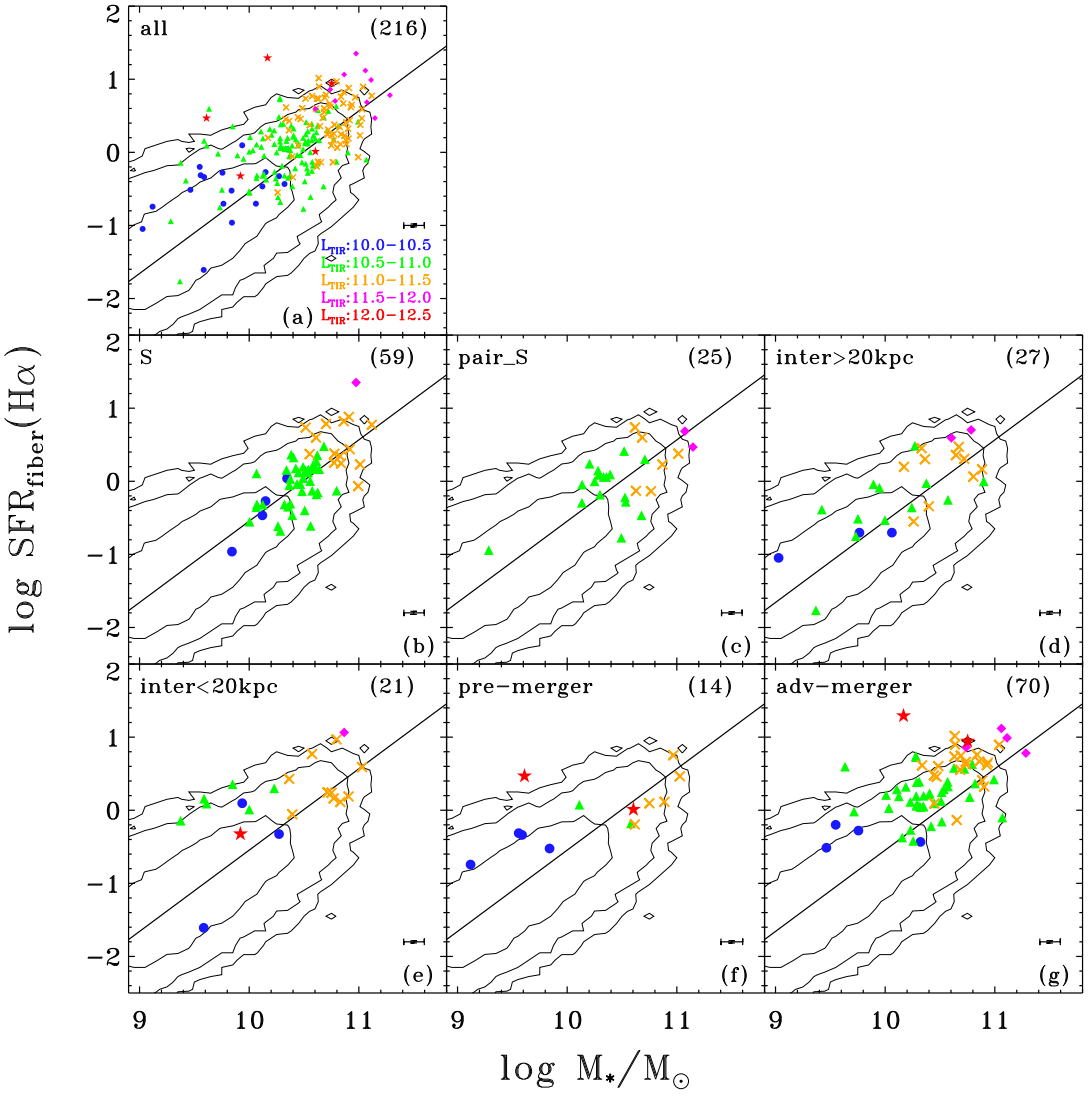

Fig. 4 Nuclear SFR versus stellar mass relation. The symbols are the same as in Figure 2 except that the black solid lines represent the nuclear SFR versus stellar mass relation defined by the control sample.

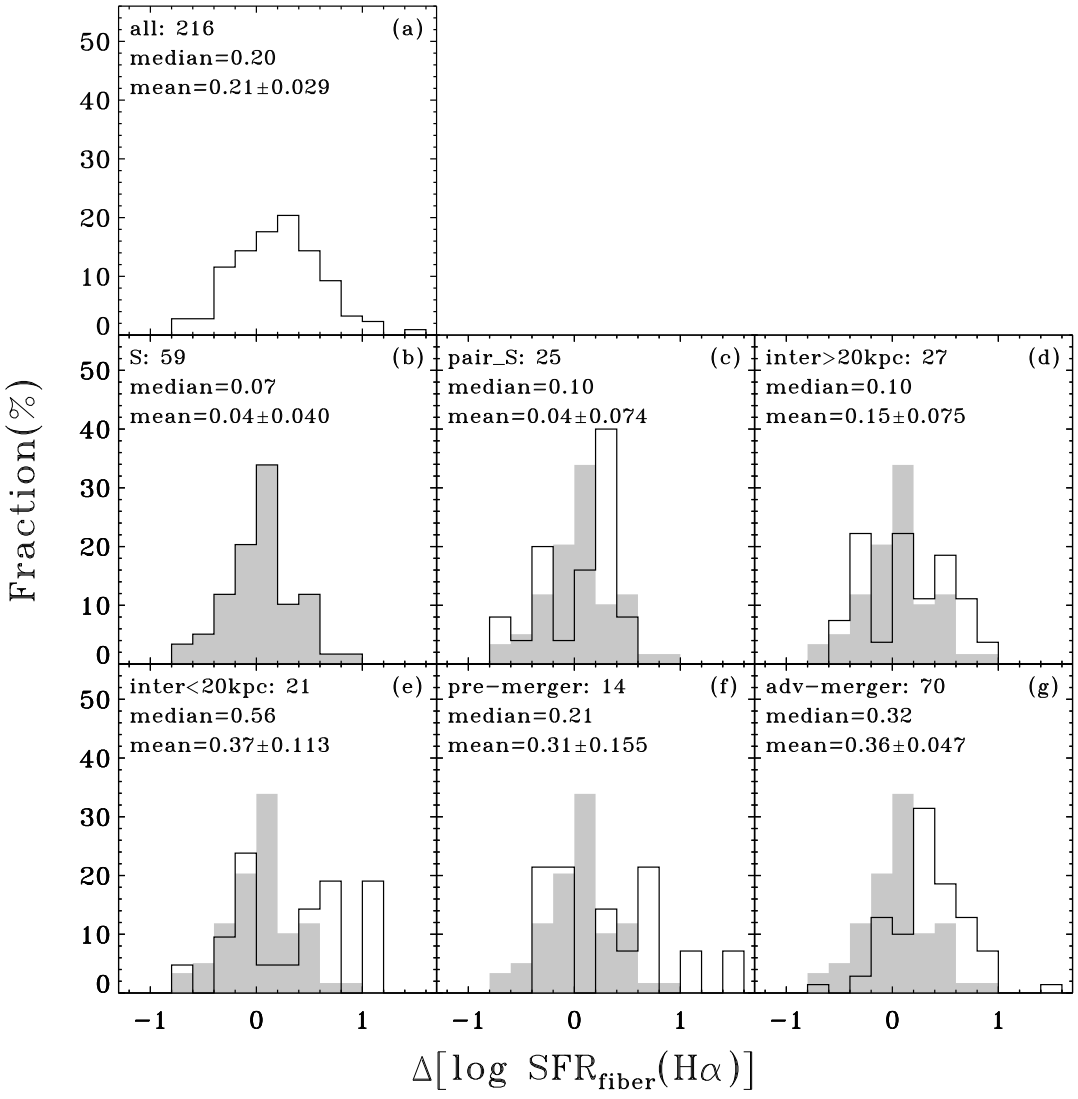

Fig. 5 Histograms of the nuclear SFR offset relative to the nuclear SFR versus stellar mass relation defined by the control sample. The histograms and legends are the same as in Figure 3 but for the nuclear SFR offset.

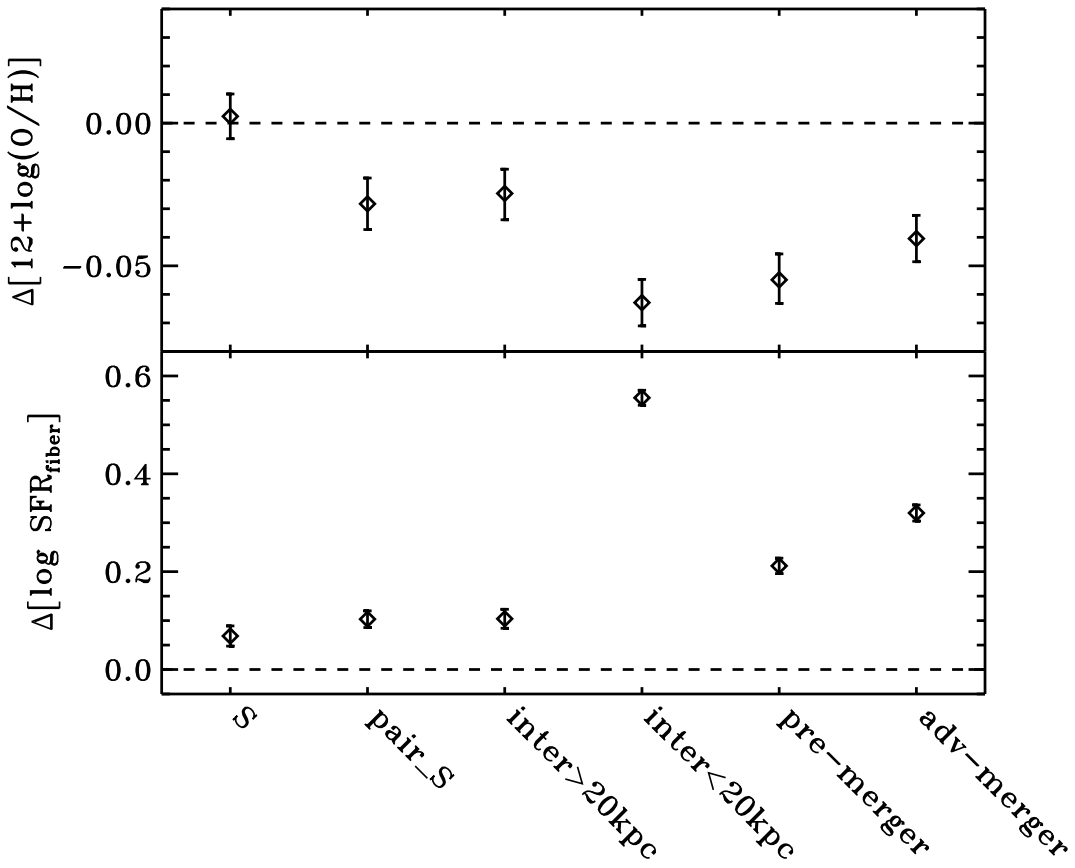

Fig. 6 Nuclear metallicity offsets (top panel) and SFR offsets (bottom panel) as a function of morphologies. Diamonds are the median offsets for galaxies within each morphological category. Error bars show the median random errors. Horizontal dashed lines indicate the line of zero offset.